Volume Title
ASP Conference Series, Vol. **Volume Number**
Author

The continuum contrast of magnetic elements as a function of magnetic field (disk center): Early studies and Hinode/SP results

P. Kobel[1], S. K. Solanki[2,3], and J. M. Borrero[4]

[1]*Max-Planck Institut für Sonnensystemforschung, Max-Planck-Straße 2, 37191 Katlenburg-Lindau, Germany*

[2]*Max-Planck Institut für Sonnensystemforschung, Max-Planck-Straße 2, 37191 Katlenburg-Lindau, Germany*

[3]*School of Space Research, Kyung Hee University, Yongin, Gyeonggi, 446-701, Korea*

[4]*Kiepenheuer-Institut für Sonnenphysik, Schöneckstr. 6, D-79110, Freiburg, Germany*

Abstract. To deepen our understanding of the role of small-scale magnetic fields on the solar irradiance, it is essential to quantify the continuum contrast of magnetic elements in the quiet Sun (QS) network and in active region (AR) plage. By using Hinode/SP disk center data at constant spatial resolution, we aimed at updating results of earlier ground-based studies of contrast vs. magnetogram signal, and to look for systematic differences between AR plages and QS network. We performed a pixel-per-pixel study of continuum contrast vs. longitudinal flux density over large fields of view in AR and in QS (as in earlier studies). Even at Hinode's resolution, the contrast of magnetic elements reaches larger values in the QS than in ARs. We show that this difference cannot be explained by different inclinations of magnetic elements in ARs and QS. We compared our contrast vs. magnetic flux density with earlier studies and attributed the differences both to our proper removal of the pores and their surrounding diffraction-spread radiation, as well as to our enhanced spatial resolution and quasi-absence of scattered light. At Hinode's resolution, the contrast of magnetic elements peaks on average at similar magnetic flux densities in ARs and in the QS, which indicates that the brightest flux tubes have similar sizes in ARs and QS.

1. Introduction

The quiet Sun (QS) network and the active region (AR) plages are the two main components of the solar photospheric magnetism outside Sunspots (Solanki et al. 2006). Both components contain small-scale magnetic features which are theoretically expected to appear bright in continuum even at disk center, the so-called "magnetic elements". As such, magnetic elements are key players in the total solar irradiance variations on the timescale of the solar cycle and shorter (Domingo et al. 2009; Krivova et al. 2003; Walton et al. 2003). It is therefore fundamental to quantify their continuum brightness in the QS network and in ARs and to investigate the underlying physics.

The brightness of magnetic features is usually measured relative to the mean intensity of the quiet photosphere, i.e. by their "contrast". The contrast at continuum

wavelengths is thus directly related to the temperature excess with respect to the quiet photosphere at the level $\tau = 1$. The temperature excess of a magnetic feature depends on its field strength (determining the depth of the opacity depression) and the radiative heating from its "hot walls" (Spruit 1976), which in turn depends on the its size (ratio of the surface of the walls to the internal volume) and, possibly, on the efficiency of the surrounding convective heat transport. Since measurements based on line-ratio techniques and inversions indicate similar field strengths in network and plages (up to a weak dependence on the filling factor, Frazier & Stenflo 1972; Stenflo 1973; Solanki & Stenflo 1984; Stenflo & Harvey 1985), the continuum contrast of magnetic features should be primarily dictated by their sizes.

To gain information about how the sizes of magnetic elements influence their contrasts, one can investigate the relation between contrast and "magnetogram signal" (i.e. net longitudinal flux density in the resolution element obtained from the calibration of Stokes V, see Stenflo 2008). Since flux tubes in QS and in AR have similar kG field strengths, the magnetogram signal scales with the fractional area of the resolution element filled by magnetic fields (see Schüssler 1992), and thus to first order with the size of the unresolved features at the line formation height. The most straightforward way to do this is to perform scatterplots of the contrast vs. magnetogram signal (cf. Frazier 1971). In spite of using the best spatial resolution at that time, it was first found that the average continuum brightness of magnetic features in ARs at disk center was never greater than the mean QS (Title et al. 1992; Topka et al. 1992). To be consistent with the theoretical expectations, the authors invoked the effect of limited resolution smearing the magnetic elements with surrounding dark moats (Title et al. 1992; Topka et al. 1992) and intergranular lanes (Title & Berger 1996). Applying the same method on QS network data (of similar resolution), Lawrence et al. (1993) nevertheless found that the average contrast was reaching positive values for some range of magnetogram signal. However, the authors could not deduce any comparison of sizes for the magnetic elements in ARs and QS, because the trend of their AR scatterplots was not peaked but instead monotonously decreasing.

2. Dataset analysis

2.1. Hinode/SP scans, maps of continuum intensity and heliocentric distance

We selected an ensemble of 6 spectropolarimetric scans over active regions and 4 scans over the quiet Sun (Hinode/SP instrument (Tsuneta et al. 2008; Suematsu et al. 2008)), performed very close to disk center. The SP delivers profiles of the four Stokes parameters (along its slit) in a visible wavelength range covering both the Fe I 630.15 nm and 630.25 nm lines, at a constant spatial resolution of 0.″3 (see e.g. Lites et al. 2008, for more details). The selected scans were performed in the "normal mode", i.e. with an exposure time of 5.8 s. All the profiles were calibrated via the `sp_prep` routine of the SolarSoft package [1]. Maps of the continuum intensity I_c (calculated in the red continuum of the 630.2 line) were provided by the `sp_prep` procedure. `sp_prep` also calculates maps of the right ascension x and declination y (heliocentric cartesian), and thereby the μ value at each pixel of the maps. In the present study, these "μ maps" were

[1] `http://www.lmsal.com/solarsoft/sswdoc/index_menu.html`

used to select exlusively portions of the scans located at the very disk center, i.e. where $\mu > 0.99$.

2.2. Inversions

The observed Stokes spectra at each spatial pixel were inverted with the VFISV (Very Fast Inversion of the Stokes Vector) code of Borrero et al. (2009) (we refer to this article for all details). This code generates synthetic Stokes profiles of the Fe I 630.1 nm line using the Milne-Eddington solution (M-E) for the radiative transfer equation (see, e.g., del Toro Iniesta 2003).

The M-E parameters of relevance for the following are: the "apparent" flux density $B_{\rm app}$, the inclination of the magnetic field vector with respect to the observer γ, and the line-of-sight (LOS) velocity plasma $v_{\rm los}$. We use the terminology "apparent" by opposition to intrinsic, in that for our purposes no filling factor treatment was performed.

All the pixels were inverted without polarization selection as the subsequent analysis will mainly deal with the longitudinal component of the flux density. The latter can be considered reliable over the range corresponding the magnetic elements where the Stokes V signal is significant, while $v_{\rm los}$ can always be considered reliable in absence of filling factor treatment (since it is determined mainly by Stokes I.).

3. Results

3.1. Scatterplots of contrast vs. of flux density for active region and quiet Sun

To start with, we performed a pixel-per-pixel comparison of continuum contrast vs. longitudinal flux density (as undertaken by Title et al. 1989; Topka et al. 1992; Lawrence et al. 1993, hereafter TTL) over active regions (ARs) and the quiet Sun (QS), to see if and how the results would differ between these two targets at the constant spatial resolution of Hinode.

Like TTL, we considered rather large fields of view (FOVs) of $70'' \times 60''$. As we obtained similar results with FOVs extracted from our different SP scans, we present here the cases of one such FOV centered on an AR plage (see Fig. 1), and one covering QS network. These FOVs were selected at the very disk center ($\mu > 0.99$).

Instead of the magnetogram signal used by TTL, we considered the unsigned (apparent) longitudinal flux density $B_{\rm app,los} = B_{\rm app}|\cos\gamma|$ (see Sect. 2.2 for $B_{\rm app}$ and γ). Like the magnetogram signal, it can be considered to scale with the size of unresolved magnetic elements (see Sect. 1). The continuum contrast in each FOV was then defined as Contrast $= \frac{I_c}{\langle I_c\rangle_{\rm QS}} - 1$, where $\langle I_c\rangle_{\rm QS}$ is the mean continuum intensity of the "quiet" pixels having $B_{\rm app,los} < 25$ Mx cm^{-2} (corresp. to rather normal granulation).

The resulting scatterplots of the continuum contrast vs. $B_{\rm app,los}$ for the AR and for QS FOVs are displayed in Fig. 2. To prevent pores to contaminate the contrasts in this range, we removed them according to the following procedure. First, their inner dark core were detected as any group of 4 pixels (minimum corresponding to spatial resolution) having contrast below -0.15 and $B_{\rm app,los} > 900$ Mx cm^{-2} (assuming pores to be resolved and thus close to kG). Next, the diffraction-spread radiation of the pores (see Sec. 3.2) was also eliminated by spatially extending the detected cores until $B_{\rm app,los}$ drops below 200 Mx cm^{-2}.

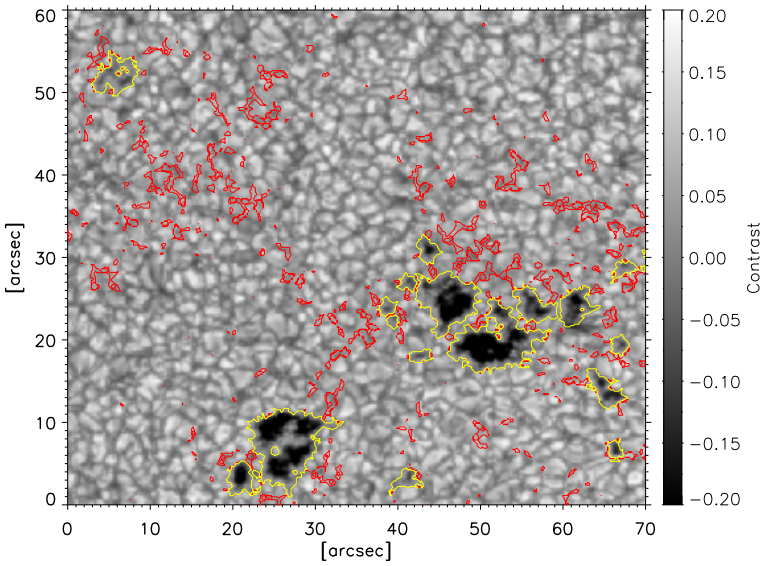

Figure 1. Continuum contrast of an active region plage area at disk center ($\mu >$ 0.99), extracted from the SP scan of day 01-02-2007. Red contours: locations of the pixels where 500 $< B_{\mathrm{app,los}} <$ 900 Mx cm^{-2}, corresponding to magnetic elements. Yellow contours: locations of the pores. The white lines across pores coincide with the locations of the cuts discussed in Sect. 3.2.

To perceive a trend within the scatterplots, the pixel contrasts were averaged into bins of $B_{\mathrm{app,los}}$ (with binwidth of 25 Mx cm^{-2}), and a third-order polynomial was fitted to the average values for $B_{\mathrm{app,los}}$ in between 200 Mx cm^{-2} and 1000 Mx cm^{-2}. The peak of the trend corresponds to "those places where the magnetic features are brightest" (Frazier71). For values of $B_{\mathrm{app,los}}$ below the peak, the features are on average less bright, either because their field strength is too low or because they are partially unresolved. For $B_{\mathrm{app,los}}$ above the peak, the features become progressively darker as their size increases and their interior are cooler. Note that unlike our trends, all the trends of TTL in ARs are monotonously decreasing. As explained in Sec. 3.2, this is not only due to our somewhat higher spatial resolution but mainly to our proper pore removal.

Two qualitative observations can be made. Firstly, even at Hinode's constant spatial resolution, the QS network reaches larger continuum contrasts on average than in AR plage. Secondly, the trends of the QS and of the AR peak at a similar value $B_{\mathrm{app,los}} \sim 700$ Mx cm^{-2}. This could not be not be noticed before since the AR trends of TTL were monotonously decreasing. This indicates that the *brightest* magnetic features in ARs and in the QS have similar sizes, which in turn poses the problem of how to explain their brightness difference.

Based on their observed center-to-limb variation of the continuum contrast of Topka et al. (1992), Lawrence et al. (1993) then proposed that the larger contrasts in the quiet Sun could be explained by a larger inclination of the magnetic elements (hot wall effect).

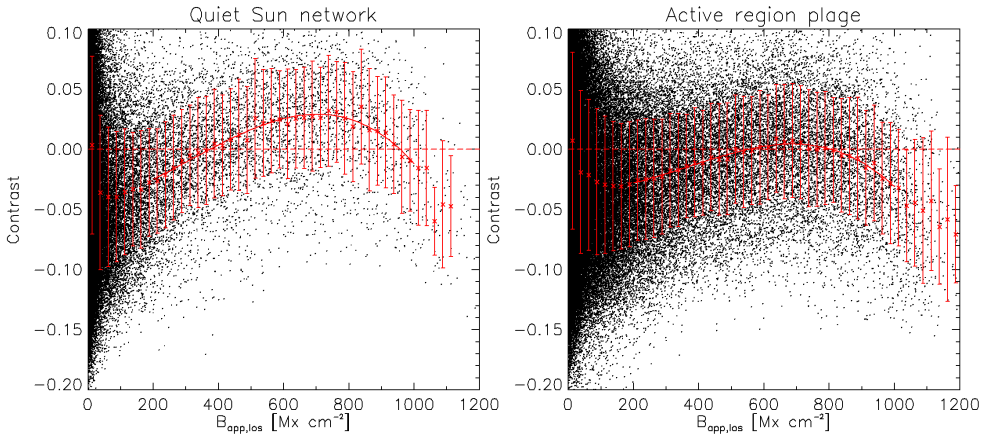

Figure 2. Scatterplot of the continuum contrast vs. longitudinal flux density $B_{\rm app,los}$ for the quiet Sun (left) and plage (right) areas, pores excluded. The contrast reference (indicated by the dashed red line) is the mean intensity of the pixels where $B_{\rm app,los} < 250$ Mx cm^{-2}. Red crosses: average values of the continuum contrast inside $B_{\rm app,los}$-bins of 25 Mx cm^{-2}. The red error bars are the standard deviations inside each bin. Solid red curve: third-order polynomial fit of the average values in the range 200 Mx cm^{-2} $< B_{\rm app,los} <$ 1000 Mx cm^{-2}.

We ruled out this possibility by studying the probability density functions (PDFs) of the inclination γ for the pixels identified with bright magnetic elements (500 Mx cm^{-2} $< B_{\rm app,los} <$ 900 Mx cm^{-2}). [2] Fig. 3 gives the example of the PDF(γ) for the plage (Fig. 1) and QS areas. The magnetic elements are close to vertical in both AR and QS, the average inclination being actually larger for the AR.

3.2. Comparison with previous studies of contrast vs. magnetogram

Here we propose possible explanations for the fact that our trends of continuum contrast averaged in bins of longitudinal flux density $B_{\rm app,los}$ are peak-shaped whereas the trends of Title et al. (1992); Topka et al. (1992); Lawrence et al. (1993) (TTL) in ARs are monotonously decreasing.

We think the main source of discrepancy is that TTL removed the pores via a simple intensity threshold. If instead of our pore removal procedure (see Sect. 3.1) we use such a contrast threshold (here taken at −0.18) on the plage area presented in Fig. 1, the resulting trend of the contrast vs. $B_{\rm app,los}$ is much flatter (see Fig. 4 left) compared to Fig. 2). This is because a simple intensity cut only removes the inner dark cores of the pores, whereas our original procedure also removes the radiation spread from the pore by diffraction. This radiation "leakage" can be seen in cuts of contrast and $B_{\rm app,los}$ across pores of different sizes, as in Fig. 5. The cuts were actually extracted from the plage area of Fig. 1 where they are marked by thick white lines. On both sides of the dark cores (identified in the cuts as having contrast < -0.18), we find several pixels where the contrast is slightly negative or neutral and $B_{\rm app,los} > 200$ Mx cm^{-2}.

[2] We checked that these pixels are relatively well located in intergranular lanes as expected for magnetic elements (see Fig. 1).

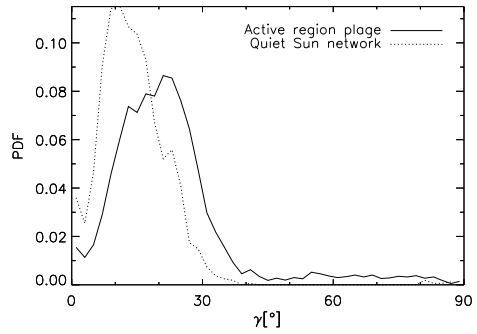

Figure 3. Probability density functions (PDFs) of the inclination γ of the magnetic elements only (500 Mx cm^{-2} < $B_{\mathrm{app,los}}$ < 900 Mx cm^{-2}) inside the quiet Sun and the active region areas.

If not removed, these pixels provide spurious contributions to the concave part of the contrast vs. $B_{\mathrm{app,los}}$ trend, with a flattening effect. For this very reason our pore removal procedure extends the detected (magnetic) dark cores of pores until $B_{\mathrm{app,los}}$ drops below 200 Mx cm^{-2}.

To further mimic the results of TTL, a degradation was necessary to adjust our scale of $B_{\mathrm{app,los}}$ to theirs. These authors indeed claim that the spatial resolution is at best 0.″3 and 0.″45 for their images and magnetograms, respectively. We actually obtained a good match to TTL's results if we degraded *both* the continuum contrast and of $B_{\mathrm{app,los}}$ with a gaussian of 0.″45 FWHM, plus an additional lorentzian degradation of 0.″06 FWHM to mimic straylight (see Fig. 4 left). The width of that lorentzian was adjusted so that the rms contrast calculated in a 20″ box of quiet Sun in our images would match the one claimed by Topka et al. (1992) (6% at 558 nm, corresponding to about 5% at 630 nm). This additional degradation implies that TTL's results are probably influenced by straylight. In contrast, the small amount of scattered light in Hinode's spectropolarimeter (Danilovic et al. 2008) can be neglected.

4. Conclusions

Even at Hinode's spatial resolution the contrast of magnetic elements (pores excluded) is on average lower in active regions (ARs) than in the quiet Sun (QS), and peaks at similar values of the longitudinal magnetic flux density for both the ARs and the QS. If the brightest magnetic elements have comparable sizes in ARs and QS (assuming a one-to-one relation between flux density and size), then another factor that could influence the heating of the magnetic elements is the efficiency of the surrounding convection, an hypothesis that will by investigated in a forthcoming paper (Kobel 2010).

Acknowledgments. We gratefully thank M. Schüssler and the ground-based solar group at the Max-Planck Institut für Sonnensystemforschung, as well as B. Vittichié and J. Sánchez-Almeida for interesting discussions about this work. This work was partially supported by WCU grant No. R31-10016 funded by the Korean Ministry of Education Science and Technology. Hinode is a Japanese mission developed and launched by ISAS/JAXA, collaborating with NAOJ, NASA and STFC (UK). Scientific

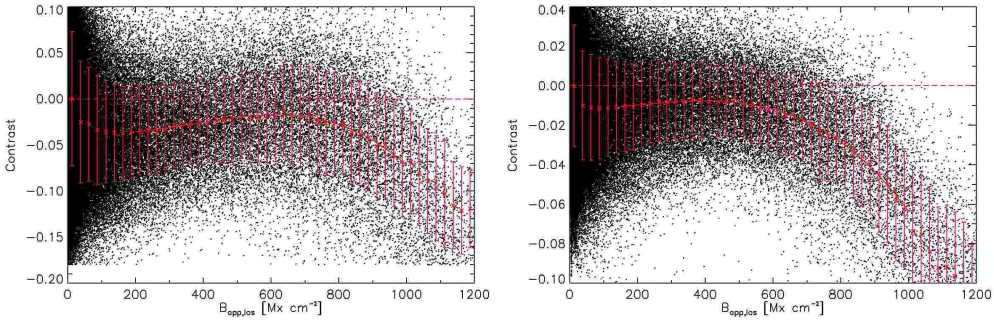

Figure 4. left: Scatterplot of the continuum contrast vs. longitudinal flux density $B_{\rm app,los}$ for the plage area shown in Fig. 1, obtained by removing the pores via a simple contrast threshold at a value of −0.18. right: Scatterplot of the continuum contrast vs. longitudinal flux density $B_{\rm app,los}$ for the plage area shown in Fig. 1, obtained after degradation of the contrast and the flux density by convolving with a gaussian of FWHM 0.″45 and a Lorentzian of FWHM 0.″06 (mimicing straylight).

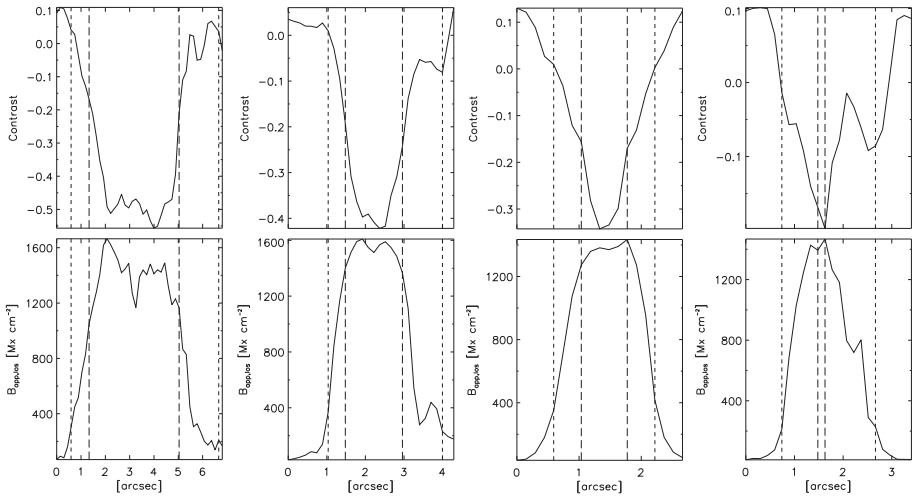

Figure 5. Contrast (upper panels) and $B_{\rm app,los}$ (lower panels) cuts across four pores of decreasing size. The long dashed lines enclose the pixels where the contrast has dropped below −0.18, and the short dashed lines delimit the pixels where $B_{\rm app,los} > 200$ Mx cm^{-2}. All cuts have been extracted from the plage area shown in Fig. 1 and their locations are indicated in that Figure by white solid lines.

operation of the Hinode mission is conducted by the Hinode science team organized at ISAS/JAXA. This team mainly consists of scientists from institutes in the partner countries. Support for the post-launch operation is provided by JAXA and NAOJ (Japan), STFC (U.K.), NASA, ESA, and NSC (Norway).

References

Borrero, J. M., Tomczyk, S., Kubo, M., Socas-Navarro, H., Schou, J., Couvidat, S., & Bogart, R. 2009, ArXiv e-prints. 0901.2702

Danilovic, S., Gandorfer, A., Lagg, A., Schüssler, M., Solanki, S. K., Vögler, A., Katsukawa, Y., & Tsuneta, S. 2008, A&A, 484, L17. 0804.4230

del Toro Iniesta, J. C. 2003, Introduction to Spectropolarimetry (by Jose Carlos del Toro Iniesta, pp. 244. ISBN 0521818273. Cambridge, UK: Cambridge University Press, April 2003.)

Domingo, V., Ermolli, I., Fox, P., Fröhlich, C., Haberreiter, M., Krivova, N., Kopp, G., Schmutz, W., Solanki, S. K., Spruit, H. C., Unruh, Y., & Vögler, A. 2009, Space Science Reviews, 145, 337

Frazier, E. N. 1971, Sol. Phys., 21, 42

Frazier, E. N., & Stenflo, J. O. 1972, Sol. Phys., 27, 330

Kobel, P. 2010, A&A. in prep

Krivova, N. A., Solanki, S. K., Fligge, M., & Unruh, Y. C. 2003, A&A, 399, L1

Lawrence, J. K., Topka, K. P., & Jones, H. P. 1993, J. Geophys. Res., 98, 18911

Lites, B. W., Kubo, M., Socas-Navarro, H., Berger, T., Frank, Z., Shine, R., Tarbell, T., Title, A., Ichimoto, K., Katsukawa, Y., Tsuneta, S., Suematsu, Y., Shimizu, T., & Nagata, S. 2008, ApJ, 672, 1237

Schüssler, M. 1992, in NATO Advanced Study Institute Series C Proc. 373: The Sun: A Laboratory for Astrophysics, edited by J. T. Schmelz, & J. C. Brown, 191

Solanki, S. K., Inhester, B., & Schüssler, M. 2006, Rep. Prog. Phys., 69, 563

Solanki, S. K., & Stenflo, J. O. 1984, A&A, 140, 185

Spruit, H. C. 1976, Sol. Phys., 50, 269

Stenflo, J. O. 1973, Sol. Phys., 32, 41

— 2008, Journal of Astrophysics and Astronomy, 29, 19

Stenflo, J. O., & Harvey, J. W. 1985, Sol. Phys., 95, 99

Suematsu, Y., Tsuneta, S., Ichimoto, K., Shimizu, T., Otsubo, M., Katsukawa, Y., Nakagiri, M., Noguchi, M., Tamura, T., Kato, Y., Hara, H., Kubo, M., Mikami, I., Saito, H., Matsushita, T., Kawaguchi, N., Nakaoji, T., Nagae, K., Shimada, S., Takeyama, N., & Yamamuro, T. 2008, Sol. Phys., 249, 197

Title, A. M., & Berger, T. E. 1996, ApJ, 463, 797

Title, A. M., Tarbell, T. D., Topka, K. P., Ferguson, S. H., Shine, R. A., & SOUP Team 1989, ApJ, 336, 475

Title, A. M., Topka, K. P., Tarbell, T. D., Schmidt, W., Balke, C., & Scharmer, G. 1992, ApJ, 393, 782

Topka, K. P., Tarbell, T. D., & Title, A. M. 1992, ApJ, 396, 351

Tsuneta, S., Ichimoto, K., Katsukawa, Y., Nagata, S., Otsubo, M., Shimizu, T., Suematsu, Y., Nakagiri, M., Noguchi, M., Tarbell, T., Title, A., Shine, R., Rosenberg, W., Hoffmann, C., Jurcevich, B., Kushner, G., Levay, M., Lites, B., Elmore, D., Matsushita, T., Kawaguchi, N., Saito, H., Mikami, I., Hill, L. D., & Owens, J. K. 2008, Sol. Phys., 249, 167. 0711.1715

Walton, S. R., Preminger, D. G., & Chapman, G. A. 2003, ApJ, 590, 1088